https://doi.org/10.5194/egusphere-2026-6470
Preprint. Discussion started: 24 November 2026
© Author(s) 2026. CC BY 4.0 License.

An evaluation of the Low Porosity Double Fence wind shield for measuring solid precipitation in Canada.

Craig D. Smith[1], Amber Ross[1], John Kochendorfer[2], Connor T. Johnson[3]

[1]Environment and Climate Change Canada, Earth System Research and Integration Division, Saskatoon, SK S7N 3H5, Canada
[2]Atmospheric Turbulence and Diffusion Division of the Air Resources Laboratory, National Oceanic and Atmospheric Administration, Oak Ridge, TN 37838, USA
[3]University of Saskatchewan, Department of Environment and Sustainability, Saskatoon, SK S7N 3H5, Canada

Correspondence to: Craig D. Smith (craig.smith@ec.gc.ca)

Abstract. The Low Porosity Double Fence (LPDF) is a precipitation gauge wind shield for improving the measurement of solid precipitation. The LPDF, designed and tested by the United States National Oceanic and Atmospheric Administration (NOAA), minimizes the wind flow around and over the precipitation gauge located in the centre of the shield to reduce wind induced undercatch during cold season operation. The configuration was originally evaluated by NOAA at three USA locations: Boulder (CO), Marshall (CO), and Chatham (MI) and was shown to improve precipitation catch efficiency to within 2% of the standard US Climate Reference Network (USCRN) precipitation measurement. However, the sites in the USA typically did not exhibit high wind speeds during solid precipitation (snow) events, with most events having a mean gauge height wind speed less than 5 m s^{-1}. To complement the NOAA evaluation, Environment and Climate Change Canada (ECCC) performed an assessment over three cold seasons (2023/2024, 2024/2025, and 2025/2026) at the Bratt's Lake precipitation intercomparison site located on the southern Canadian Prairies where the mean gauge height wind speed during solid precipitation events is about 5 m s^{-1} with many events exhibiting wind speeds exceeding 8 m s^{-1}. At Bratt's Lake, the LPDF performance is compared to the World Meteorological Organization (WMO) Double Fence Automated Reference (DFAR) as well as other common wind shield configurations such as the single Alter (SA) and double Alter (DA). Intercomparison results showed that the LPDF outperformed the SA and DA shields, increasing the relative total catch (RTC) of cold season (October through April) total precipitation to 77% of the WMO reference, an improvement over the 67% and 72% RTC demonstrated by the SA and DA gauges (respectively). For solid precipitation, the LPDF achieved an RTC of 74%, resulting in a 20% increase relative to the SA gauge. The performance of the LPDF demonstrated by the NOAA evaluations could not be replicated in the colder and windier conditions experienced at Bratt's Lake. This necessitates the development of transfer functions for adjusting the wind induced undercatch experienced by the LPDF if this configuration is to be used for measuring cold season precipitation in Canada.

https://doi.org/10.5194/egusphere-2026-6470
Preprint. Discussion started: 24 November 2026
© Author(s) 2026. CC BY 4.0 License.

1 Introduction

The accurate measurement of precipitation is critical for many applications including climate monitoring (Vincent et al., 2018), climate trend analysis (Vincent & Mekis, 2006), water resource forecasting (Pomeroy et al., 2007; Barnett et al., 2005), and numerical weather prediction assimilation and verification (Lespinas et al., 2015; Buisan et al., 2020; Køltzow et al., 2020). It is also well documented that automated precipitation gauges operated in cold regions are prone to under-measuring solid precipitation (snow) because their design allows wind to deflect lighter snow particles away from the collector inlet, the severity of which is dependent on the configuration of the gauge and wind shield (if used) and the environmental conditions (temperature and wind speed) during which the measurement is made (Sevruk et al., 1991; Goodison et al., 1998; Nitu et al., 2018). Kochendorfer et al. (2017b) indicated that the shield configuration around the gauge affects solid precipitation catch efficiency (CE) much more than the model of the gauge being used and showed the relative decrease in CE with increasing wind speed and decreasing temperature for shielded and unshielded automated gauges. The intercomparison of multiple gauge and shield configurations during the World Meteorological Organization (WMO) Solid Precipitation Inter-Comparison Experiment (SPICE) showed that more significant shielding (i.e. double shielding vs. single shielding vs. no shielding) increased the solid precipitation CE for a given wind speed (Nitu et al., 2018) and slowed the rate of decrease in CE with increasing wind speed. This was documented further by Kochendorfer et al. (2022).

The main advantage of increased shielding when measuring solid precipitation is that higher CE means lower bias errors and more accurate measurements. To adjust precipitation for wind bias, it has been shown by Kochendorfer et al. (2018) that the uncertainty in the adjusted observation increases as a function of the magnitude of the adjustment factor, so the high gauge CE reduces that uncertainty. Furthermore, when solid precipitation values are adjusted for wind bias, users are often unaware that a significant number of light events occurring during cold and windy conditions may go fully undetected by the precipitation gauge, and when this occurs, unobserved precipitation amounts cannot be adjusted via conventional transfer functions. Smith et al. (2020) showed that an unshielded automated gauge at the Bratt's Lake WMO-SPICE site completely missed a significant number of events accumulating to 24% of the total cold season (October through April) precipitation measured by the co-located WMO-SPICE reference measurement. Using a single Alter shield reduced this occurrence to 14% of the reference-measured total cold season precipitation, and it is anticipated that more shielding would further decrease this error by increasing the detectability of light snow events. By extension, increased detectability also increases the effectiveness of applied transfer functions to adjust observed precipitation to be closer to the true amount.

The current WMO reference gauge configuration for the automated measurement of solid precipitation is the Double Fence Automated Reference (DFAR; Nitu et al., 2018) which consists of an automated gauge housed inside a large octagonal double fence. The double fence structure is identical to that used for manual precipitation gauge measurements during the first WMO Solid Precipitation Intercomparison (Goodison et al., 1998) where it was called the Double Fence Intercomparison Reference

https://doi.org/10.5194/egusphere-2026-6470
Preprint. Discussion started: 24 November 2026
© Author(s) 2026. CC BY 4.0 License.

or DFIR. The manual DFIR, using a Tretyakov gauge, was originally tested at Valdai Russia (1970-1990) and shown by Yang et al. (1993) to perform satisfactorily with only small differences in CE as compared to previous solid precipitation measurement references (such as a naturally bush-shielded gauge). Intercomparisons prior to WMO-SPICE showed close interoperability between the DFIR and what would become the DFAR (Nitu et al., 2018). The advantage of the DFIR and the DFAR wind shield is that the CE of solid precipitation remains relatively high as wind speed increases (Yang et al., 1993). The disadvantage of the DFIR and DFAR is the large footprint required for construction and operation: the outer fence of a DFAR shield has a diameter of 12 m and a height of 3.5 m and the inner fence has a diameter of 4 m and a height of 3 m. The wind fence construction cost (labour and materials) is substantial as is the maintenance, especially where conditions are more extreme. Although WMO-SPICE recommends that climate observation networks operate at least one DFAR for intercomparing and qualifying automated precipitation gauges, wide scale use of the DFAR in observation networks is neither practical nor cost effective.

1.1 The Low Porosity Double Fence

The design and evaluation of a new reference precipitation gauge wind shield is described by Kochendorfer et al. (2023), henceforth known as K2023. This new wind shield design is significantly smaller than the DFAR but with lower porosity of ~25% than the ~50% porosity of the DFAR. Named the Low Porosity Double Fence (LPDF), this new fence structure consists of an octagonal shaped outer fence with a diameter of about 5 m and a square inner fence with dimensions close to 2 m. Like the DFAR, the heights of the outer and inner fences are staggered in relation to the height of the gauge in the centre, with the outer (inner) fence being approximately 40 cm (20 cm) above the orifice of the gauge. Exact dimensions are provided by K2023. Vinyl privacy slats are inserted into the chain link fence panels to effectively decrease the porosity available for air to flow through the panels. Photos of the LPDF are shown in Section 2 (Fig. 5).

Besides having a relatively small footprint, the LPDF is constructed from commercially available chain link fence panels and hardware and is virtually maintenance free. According to K2023, the smaller footprint, lower maintenance, and relatively easy installation make the configuration a viable option for the United States Climate Reference Network (USCRN) which currently uses a modified two-thirds scale version of the DFAR called the Small DFIR (or SDFIR). The reported cost of materials for the LPDF is approximately $2000 USD, representing a fraction of the cost of materials and labour required for a SDFIR or a DFAR.

According to K2023, three sites in the USA that were selected for the LPDF evaluation: Boulder (CO), Marshall (CO), and Chatham (MI). Each site had a co-located SDFIR (Marshall having an automated “DFIR-shielded gauge” which will be referred to as a DFAR henceforth) and ancillary meteorological measurements (including wind speed at 3 m and 10 m and air temperature at 1.5 m). In general, the total (all phase) precipitation as measured by the LPDF, over nearly 3 years, differed by less than 1% of that measured by the SDFIR. At Marshall, the LPDF measured 1.4% less solid precipitation than the DFAR.

https://doi.org/10.5194/egusphere-2026-6470
Preprint. Discussion started: 24 November 2026
© Author(s) 2026. CC BY 4.0 License.

However, wind speeds at each of these sites on "snow days" (defined by K2023 as a 24-hour period when precipitation > 1 mm and mean temperature < -2° C) are considered light to moderate, with the number of snow days with wind speed < 5 m s^{-1} where observed precipitation values relative to the WMO standard range from >75% at Boulder to > 95% at Marshall.

1.2 Objectives

Given the favourable intercomparison between the LPDF and the SDFIR at the NOAA test sites and between the LPDF and the DFAR at Marshall, Environment and Climate Change Canada (ECCC) opted to test the LPDF over several winter seasons in the Canadian context, specifically at an exposed site on the Canadian Prairies where cold season precipitation occurs at relatively low temperatures and at relatively high wind speeds. Although ECCC does not normally operate the SDFIR, an intercomparison between the LPDF and the DFAR will provide a gauge configuration performance assessment like those achieved during WMO-SPICE. The objective is to determine the performance of the LPDF as compared to the DFAR, including a wind speed-temperature-CE relationship (a.k.a. a transfer function), and to put the LPDF performance into context relative to other wind shield configurations evaluated during WMO-SPICE in a moderately extreme winter environment. Finally, a recommendation is made regarding the use and operation of the LPDF, either as a reference or as a standard configuration, in Canadian (or similar) cold season conditions.

2 Methods

2.1 Study site

The Bratt's Lake precipitation intercomparison supersite (Fig. 1; 50.200° N, 104.711° W) operated by ECCC is a WMO-SPICE site (Nitu et al., 2018) located on the exposed Canadian Prairie. The intercomparison site has been in operation by ECCC since 2003 and was selected for precipitation gauge intercomparisons because of the relatively cold dry winters which experience high wind speeds during cold season precipitation events. The mean gauge height wind speed and temperature experienced during cold season precipitation events (October through April, calculated over the 2020-2025 period) is 6.0 m s^{-1} and -10.5 °C. The site often experiences wind speeds during winter precipitation events exceeding 8 m s^{-1} (Fig. 2). These conditions produce a moderate to severe environment for solid precipitation measurement. Using the Kochendorfer et al. (2017b) CE analysis, an unshielded precipitation gauge would experience a mean undercatch of 71% in those conditions.

https://doi.org/10.5194/egusphere-2026-6470
Preprint. Discussion started: 24 November 2026
© Author(s) 2026. CC BY 4.0 License.

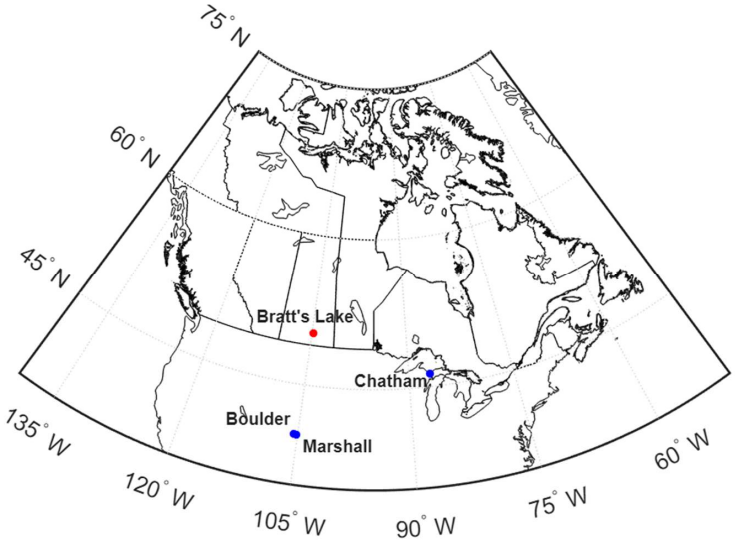

Figure 1: Location of the ECCC Bratt's Lake study site (red) as well as the three NOAA USA test sites (blue) from K2023.

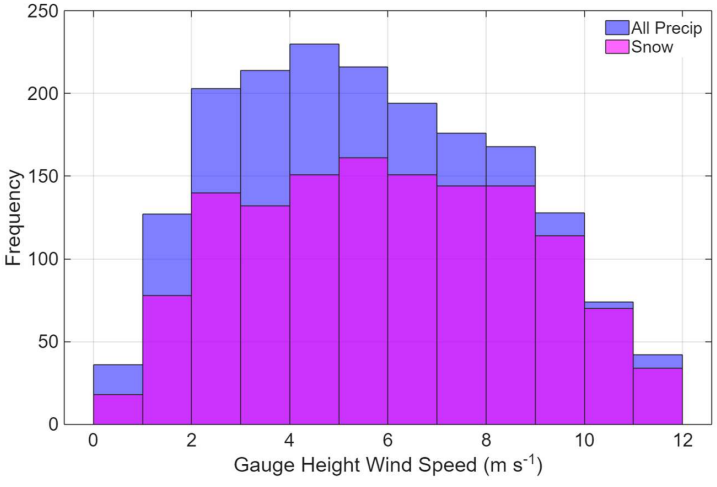

Figure 2: Frequency of occurrence of the magnitude of hourly mean gauge height wind speeds during cold season (October through April) precipitation events (blue) and during solid precipitation events (magenta) as measured by the DFAR over the 2020-2025 winter periods at Bratt's Lake.

https://doi.org/10.5194/egusphere-2026-6470
Preprint. Discussion started: 24 November 2026
© Author(s) 2026. CC BY 4.0 License.

2.2 Instrumentation

The Bratt's Lake site, shown to scale in the site diagram (including pedestal labels) in Fig. 3, is equipped with two DFAR gauge configurations (East and West, pedestals A1 and Z1 respectively) that served as reference configurations during the WMO-SPICE project. The East DFAR (Fig. 3a) houses a Geonor T-200B precipitation gauge (with rim heating) and serves as the reference for this intercomparison. The site also supports a single Alter-shielded (SA) Geonor T-200B (GeonorSA; Fig. 4b, pedestal B2) that until recently was the standard precipitation gauge configuration in the ECCC operational surface network (Mekis et al., 2018). There are also multiple double Alter-shielded (DA) OTT Pluvio^{2}L (P2LDA) gauges (Fig. 4c, pedestals B5, C1, and C4) installed that represent the current standard ECCC precipitation gauge configuration. None of the SA or DA shielded gauges currently use rim heating. Ancillary meteorological data include wind speed and direction (pedestal A4) at gauge height (~2.2 m) and at 10 m and aspirated 1.5 m air temperature in a Stevenson screen.

The LPDF (Fig. 5, pedestal D5) is installed around a Geonor T-200B (with rim heating). The shield was built using the K2023 specification with some minor modifications such as ground anchors to hold the structure in place during high winds. Rim heating protocols are the same as for the DFAR and are consistent with those used during WMO-SPICE (Nitu et al., 2018). That is, rim heating is toggled via imbedded thermistors to try to maintain a rim temperature of 2 °C. However, ambient conditions and available heating power often prevent the rim temperature from achieving 2 °C when air temperature is below -5 °C and when wind speeds are relatively high, but a rim temperature higher than air temperature is almost always attainable.

https://doi.org/10.5194/egusphere-2026-6470
Preprint. Discussion started: 24 November 2026
© Author(s) 2026. CC BY 4.0 License.

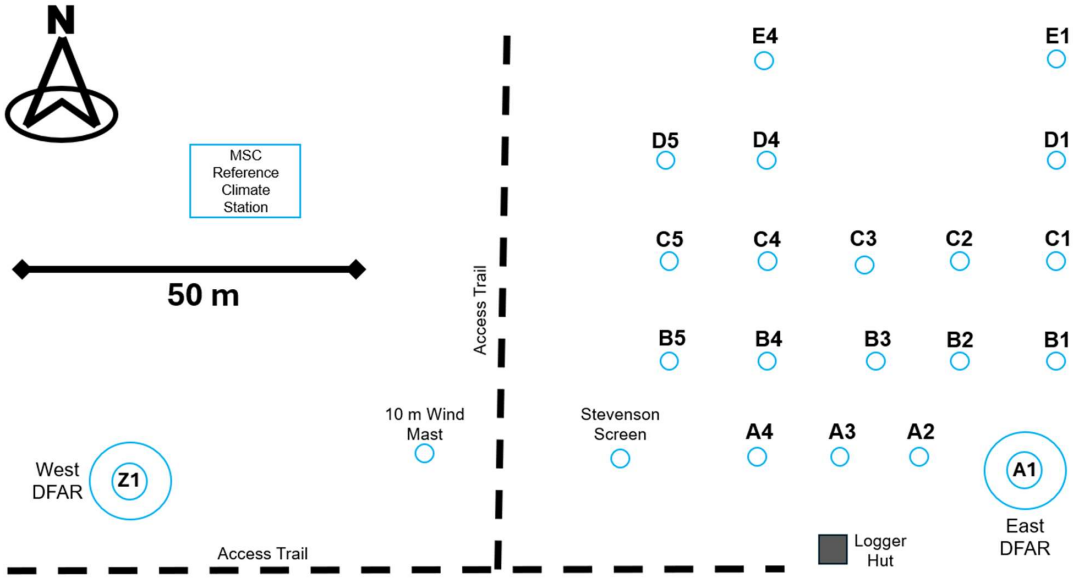

Figure 3: Bratt's Lake site diagram (drawn to scale). The DFAR used as the reference is installed at A1, the LPDF at D5, the GeonorSA at B2, and the P2LDA at C4.

145

https://doi.org/10.5194/egusphere-2026-6470
Preprint. Discussion started: 24 November 2026
© Author(s) 2026. CC BY 4.0 License.



Figure 4: Bratt's Lake precipitation gauges and wind shields: a) the Double Fence Automated Reference (DFAR) on pedestal A1, b) single Alter-shielded Geonor T-200B (GeonorSA) on pedestal B2, and c) double Alter-shielded Pluvio^{2}L (P2LDA) on pedestal C4.

150

https://doi.org/10.5194/egusphere-2026-6470
Preprint. Discussion started: 24 November 2026
© Author(s) 2026. CC BY 4.0 License.







Figure 5: The Low Porosity Double Fence (LPDF) configuration: a) exterior view after completing installation with the vinyl inserts at Bratt's Lake (pedestal D5) and b) exterior view prior to installation of the vinyl inserts at Bratt's Lake, and c) high angle view of a NOAA LPDF during design and original construction.

https://doi.org/10.5194/egusphere-2026-6470
Preprint. Discussion started: 24 November 2026
© Author(s) 2026. CC BY 4.0 License.

2.3 Data collection and quality control

All data were collected at a frequency of one-minute over three winters seasons: October through April 2023/2024, 2024/2025, and 2025/2026. For configurations using the Geonor T-200B precipitation gauge (DFAR, GeonorSA, and the LPDF), the raw one-minute data consisted of gauge bucket weight measurements derived from three vibrating wire transducers. The three bucket weights were then averaged over one hour and filtered for noise using the ECCC supervised NAF-S filter (Ross et al., 2020) but not before large data artifacts (e.g. due to gauge servicing) were removed manually. The P2LDA produced several data outputs, but the data used here were from the one-minute real-time bucket weight output filtered using NAF-S. Following noise filtering, interval precipitation amounts were calculated as the increase in the filtered bucket weight over the interval. The one-minute air temperature and wind data were quality controlled using the WMO-SPICE procedure (Nitu et al., 2018). Finally, data were amalgamated to a temporal resolution of one-hour. Hourly precipitation (mm) totals were derived as the sum of the one-minute interval amounts. Hourly gauge height wind speed (U_{gh}, m s^{-1}) and air temperature (T_{air}, °C) data were derived as a mean of the quality controlled one-minute data over the same hour as the precipitation accumulation. If 6 or more one-minute values (10%) are missing in any of the parameters, the entire hour was set to missing.

As reported by K2023 and Nitu et al. (2018), uncertainties due to random errors in the gauge measurement of precipitation accumulation at short time intervals (i.e. one-minute to 30-minute) using different gauge and shield configurations make it difficult to compare performances. This difficulty is often exacerbated by noise filtering, such as NAF-S, which may distribute precipitation during periods of high signal noise into adjacent accumulation intervals (i.e. plus or minus one or more hours from the time that the precipitation occurred). To avoid this, performance is often assessed by plotting accumulated time series. Smith et al. (2020) introduced the Relative Total Catch (RTC) metric for intercomparing gauge configuration performance, which is simply the ratio of the total precipitation over the study period measured by the configuration under test to the total precipitation measured by the reference and expressed as a percentage. As in K2023, Smith et al. (2020) and previous WMO-SPICE analysis (Wolff et al., 2015; Nitu et al., 2018) where estimating precipitation phase is required for analysis, it was determined via temperature banding so that precipitation is considered solid at $T_{air} < -2$ °C, liquid at $T_{air} > 2$ °C, and mixed for $2\ °C \geq T_{air} \geq -2\ °C$.

During the 2024/2025 winter, some construction work at the site required snow to be pushed away from the work area and resulted in ~2 m high windrow obstruction at 20 m to 30 m North and Northwest of the LPDF installation (Fig. 3, D5). It was suspected that loose snow was blowing off these windrows and potentially impacting the precipitation measured by the nearby gauges (the LPDF and the P2LDA being the closest). For this reason, the precipitation data collected during the winter of 2024/2025 was filtered to remove occurrences of precipitation when the wind direction at gauge height was in the 260° to 360° range. As part of the process to aggregate the data from one-minute to hourly, mean hourly wind directions were calculated via vectorized averaging, and hourly data within the masked 260° to 360° wind direction range were removed. However, there

https://doi.org/10.5194/egusphere-2026-6470
Preprint. Discussion started: 24 November 2026
© Author(s) 2026. CC BY 4.0 License.

remained a concern of a significant contribution by blowing snow to hourly precipitation when the wind was from the direction of the windrows even after filtering using the hourly means. This was examined further by using data aggregation and vector magnitude analysis to determine the contribution of remaining one-minute wind occurrences from the windrow direction to the hourly means. The analysis showed that when there were 10 or fewer one-minute observations of wind direction from the windrows included in the hourly mean, the contribution of these data to the one-hour means were less than 15%. It was therefore decided to further filter the hourly data if more than 10 occurrences of one-minute wind direction from the masked range were included in the hourly mean. Of the 5088 hours of data during the 2024/2025 winter season, 2328 hours were removed accounting for approximately 42% of the seasonal precipitation total (as measured by the DFAR). This filtering exercise increased the confidence that precipitation measured by the gauges closer to the disturbed snow were not biased due to blowing snow. In addition, intercomparison of precipitation data only included the hours where there were no missing measurements from all four precipitation gauge configurations. This means that the analysed precipitation totals for the 2024/2025 season do not accurately reflect the total precipitation received at the site.

It also needs to be noted that the rim heater relay for the LPDF failed during the 2025/2026 season so that the rim heater was continuously on, resulting in rim temperatures significantly higher than 2 °C when conditions allowed. Although this was repaired following the discovery of the issue, the beginning of the 2025/2026 data were omitted from our analysis and therefore the 2025/2026 accumulation period began January 14th of 2026. Removing the start of the season impacted the 2025/2026 seasonal totals and means, and this should be considered when putting this season into context with the other seasons.

2.4 Catch efficiency and transfer function development

Shorter aggregation periods are necessary for the development of a TF using methods described by Kochendorfer et al. (2017a, 2017b). For these periods, there is often a compromise between increased random error associated with short precipitation accumulation periods and the loss of representativeness of the meteorological conditions during the time periods (Nitu et al., 2018). However, using time periods that are too short reduces the amount of measurable low-rate or light precipitation that can be included for analysis. The compromise is to use a 60-minute aggregation for TF development rather than the 30-minute periods used by Kochendorfer et al. (2017a, 2017b, 2018). However, these methods are otherwise similar to those used by Kochendorfer et al. (2017a, 2017b) which allows for some comparison between existing TF curves for different gauge configurations.

Starting with the three combined seasons of aggregated 60-minute data, the precipitation data is filtered so that only DFAR measured events ≥ 0.250 mm and LPDF events ≥ 0.169 mm are used for calculating the CE. The LPDF threshold of 0.169 mm is calculated as the median of the ratios of the LPDF to the DFAR precipitation totals when air temperature is < -5 °C and 10 m wind speed is > 5 m s^{-1}, which is then multiplied by the DFAR threshold (referred to as the $THOLD_{UT}$ by Kochendorfer et

https://doi.org/10.5194/egusphere-2026-6470
Preprint. Discussion started: 24 November 2026
© Author(s) 2026. CC BY 4.0 License.

al., 2017b). The events were further filtered to remove high wind speeds (U_{gh} > 10 m s^{-1}) to reduce the impact of blowing snow. Unlike the WMO-SPICE methodology, no present weather detector threshold was used for verifying occurrence, but this is partially compensated for by using 60-minute accumulations rather than shorter intervals as was done for WMO-SPICE. CE was then used to fit Eq. (1) (from Kochendorfer et al., 2017b) using the 60-minute mean gauge height wind speed (U_{gh} in m s^{-1}) and 1.5 m aspirated air temperature (T_{air} in °C). Equation (1), where a, b, and c are the coefficients that fit the data to the model, is a temperature continuous function that does not require pre-determined precipitation phase:

$$CE = e^{-a(U_{gh})(1-\tan^{-1}(b(T_{air}))+c)}, \quad (1)$$

3 Results and Discussion

3.1 Data summary

Table 1 summarizes the three intercomparison seasons, showing seasonal and combined DFAR measured total (all types) precipitation (P_{DFAR} Total) and DFAR measured solid precipitation (P_{DFAR} Snow), as well as the total number of events for each category. Mean air temperature (T_{air}) and gauge height wind speeds (U_{gh}) during all precipitation are also shown for each category. Total combined precipitation, after 2024/2025 was filtered for wind direction, and due to the late start to the 2025/2026 season due to sensor malfunction, was 304 mm and 176 mm of total precipitation and solid precipitation respectively. The combined wind speed mean was 3.7 m s^{-1}, increasing to 5.4 m s^{-1} for solid precipitation events. The 2025/2026 season, because of the mid-January start date, shows a lower mean temperature for all precipitation and higher mean wind speeds for total precipitation and for solid precipitation. Despite the shorter season, 2025/2026 had the highest solid precipitation accumulation of the three seasons.

Table 1: Mean meteorological conditions during all (Total) precipitation and during solid precipitation (Snow) broken down by season and for the three seasons combined. P_{DFAR} is precipitation measured by the DFAR, n is the number of hourly events, U_{gh} is the mean wind speed measured at gauge height during precipitation, and T_{air} is mean air temperature measured at 1.5 m above the ground during precipitation.

Season	P_{DFAR} Total (mm)	n	P_{DFAR} Snow (mm)	n Snow	U_{gh} (m s^{-1})	U_{gh} Snow (m s^{-1})	T_{air} (°C)	T_{air} Snow (°C)
2023/2024	137	310	50	183	3.8	5.2	-3.6	-11.3
2024/2025*	82	174	54	127	3.1	5.1	-4.9	-13.5
2025/2026**	85	196	72	175	4.1	6.0	-5.7	-8.3
Combined	304	680	176	485	3.7	5.4	-4.7	-11.0

* does not include hourly data within the masked wind direction range, ** season begins January 14, 2026

https://doi.org/10.5194/egusphere-2026-6470
Preprint. Discussion started: 24 November 2026
© Author(s) 2026. CC BY 4.0 License.

245

3.2 Time series and RTC

Figures 6 and 7 show the accumulated time series for the three winter seasons for the LPDF (magenta), DFAR (black), P2LDA (green) and the GeonorSA (blue) for all precipitation and for solid precipitation (respectively). Tables 2 and 3 provide the precipitation summaries for each of the gauge configurations for total precipitation and for solid precipitation respectively.
250 The tables also provide the RTC calculations expressed as a percentage.

The accumulated time series shows a consistent trend with the DFAR measuring the most precipitation for all three seasons followed by the LPDF, P2LDA, and the GeonorSA. Solid precipitation dominates the intercomparison periods (about 58% of the total amount and 71% of the events). The differences in the amount of precipitation between the configurations is typically
255 more pronounced for solid precipitation (Fig. 7) than it is for total precipitation (Fig. 6). This is reflected in the combined RTC in that the difference between the GeonorSA and the LPDF increases from 10% for total precipitation to 20% for solid precipitation, highlighting the relative effectiveness of more substantial shielding to increase the CE for solid precipitation in this environment. The LPDF increases the RTC for solid precipitation by 13% over the P2LDA, although only achieves a mean RTC of 74% (77%) for solid (total) precipitation.

260

A *t*-test was used to determine if there was a significant difference between the LPDF and DFAR precipitation mean with p=0.003 and t-statistic = -3.0. The difference was even more significant for solid precipitation ($p < 0.001$ and t-statistic = -3.5).

265 **Table 2: Total precipitation amounts (P_{total}) and relative total catch (RTC) compared to the DFAR for each gauge configuration.**

Configuration	2023/2024		2024/2025*		2025/2026**		Combined	
	P_{total} (mm)	RTC (%)	P_{total} (mm)	RTC (%)	P_{total} (mm)	RTC (%)	P_{total} (mm)	RTC (%)
DFAR	137	-	82	-	85	-	304	-
LPDF	111	81%	62	76%	62	73%	235	77%
P2LDA	103	75%	60	73%	56	66%	219	72%
GeonorSA	98	72%	54	66%	51	60%	203	67%

* does not include hourly data within the masked wind direction range

** season begins January 14, 2026

270

https://doi.org/10.5194/egusphere-2026-6470
Preprint. Discussion started: 24 November 2026
© Author(s) 2026. CC BY 4.0 License.

Table 3: Solid precipitation amounts (P_{snow}) and relative total catch (RTC) compared to the DFAR for each gauge configuration.

Configuration	2023/2024		2024/2025*		2025/2026**		Combined	
	P_{snow} (mm)	RTC (%)	P_{snow} (mm)	RTC (%)	P_{snow} (mm)	RTC (%)	P_{snow} (mm)	RTC (%)
DFAR	50	-	54	-	71	-	175	-
LPDF	35	70%	40	74%	54	76%	129	74%
P2LDA	30	60%	35	65%	42	59%	107	61%
GeonorSA	27	54%	28	52%	39	55%	94	54%

275 * does not include hourly data within the masked wind direction range

** season begins January 14, 2026

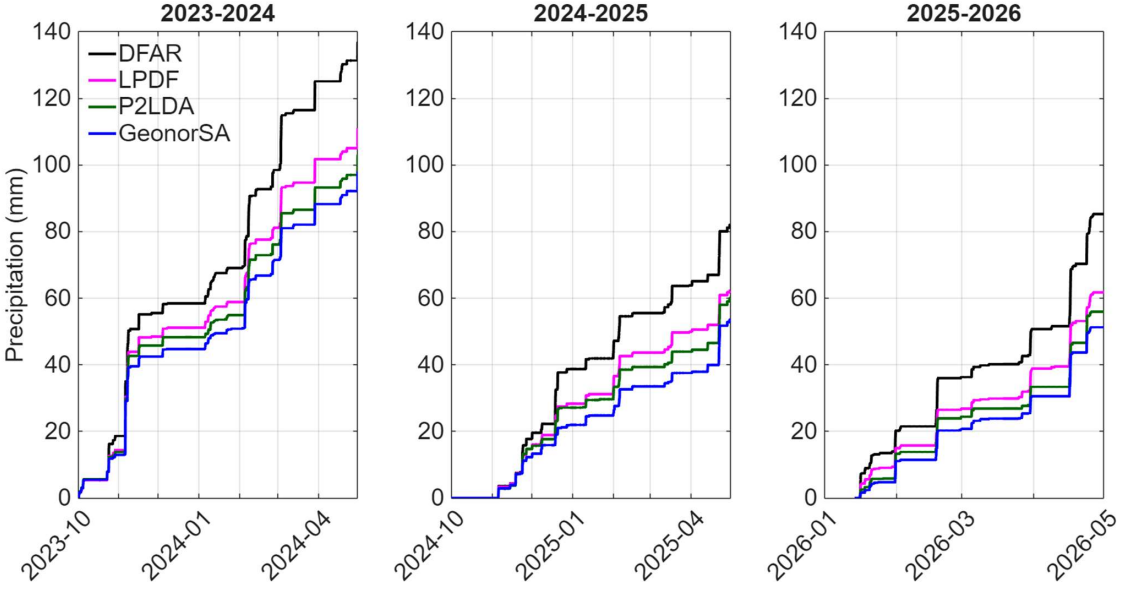

Figure 6: Accumulated total precipitation time series intercomparison for 2023/2024 (left), 2024/2025 (middle), and 2025/2026 (right) for the LPDF (magenta), DFAR (black), P2LDA (green), and GeonorSA (blue). Note that the 2024/2025 precipitation is

https://doi.org/10.5194/egusphere-2026-6470
Preprint. Discussion started: 24 November 2026
© Author(s) 2026. CC BY 4.0 License.

filtered to remove events occurring when wind direction is between 260° and 360° and that the accumulation for 2025/2026 doesn't begin until mid-January 2026.

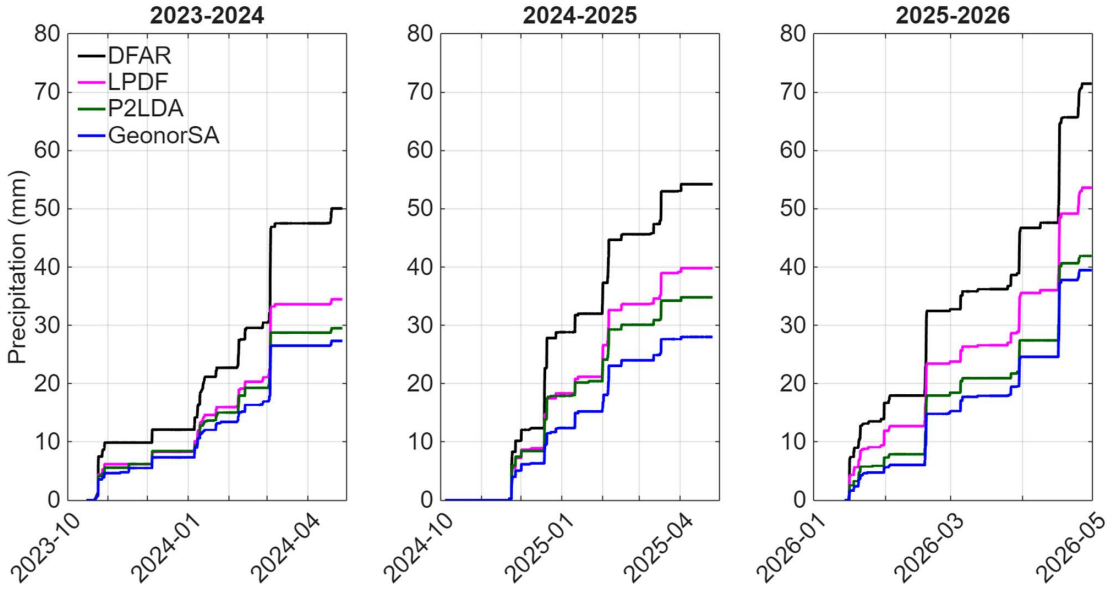

Figure 7: Accumulated solid precipitation time series intercomparison for 2023/2024 (left), 2024/2025 (middle), and 2025/2026 (right) for the LPDF (magenta), DFAR (black), P2LDA (green), and GeonorSA (blue). Solid precipitation is determined as precipitation occurring when hourly mean Tair is less than -2 °C. Note that the 2024/2025 precipitation is filtered to remove events occurring when wind direction is between 260° and 360° and that the accumulation for 2025/2026 doesn't begin until mid-January 2026.

3.3 Catch efficiency and transfer functions

280 The CE for the LPDF was calculated using the pre-described methodology, classified as solid precipitation, mixed precipitation, and rain using temperature, and plotted against gauge height wind speed (U_{gh}) in Fig. 8. Even with considerable scatter, there is a distinct decrease in the LPDF CE with increasing wind speed for both solid (blue) and mixed (grey) precipitation. Regression analysis (not shown) produces a slope of -0.04 (Solid) to -0.05 (Mixed) but with r^2 values under 0.30.

285

https://doi.org/10.5194/egusphere-2026-6470
Preprint. Discussion started: 24 November 2026
© Author(s) 2026. CC BY 4.0 License.

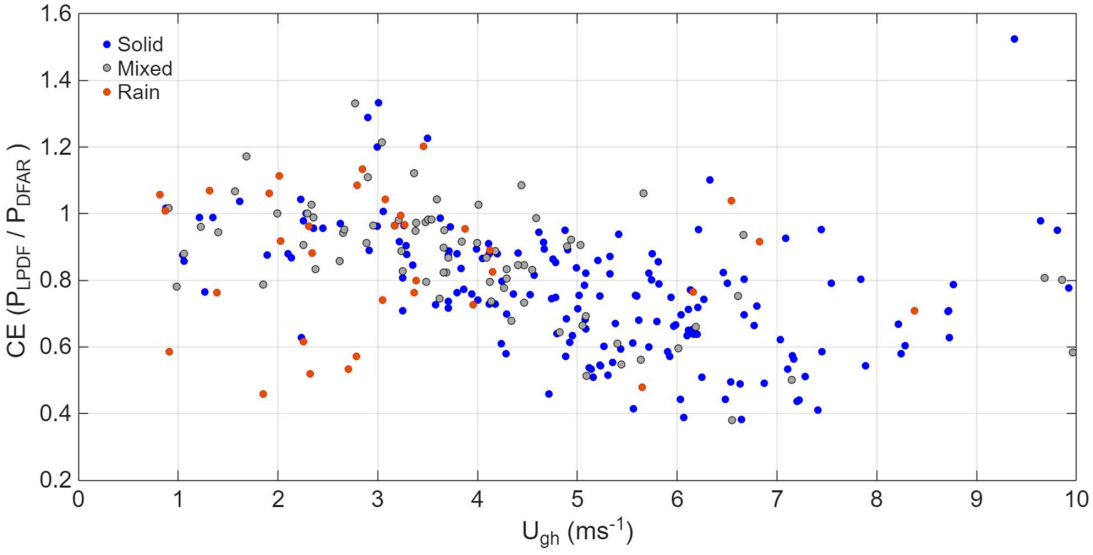

Figure 8: LPDF Catch Efficiency (CE) vs. gauge height wind speed (U_{gh}) for solid precipitation (blue), mixed precipitation (grey) and rain (red).

Fitting the CE data shown in Figure 8 (excluding CE > 1.2) to Eq. 1, where CE = $f(T_{air}, U_{gh})$, results in the coefficients *a*, *b*, and *c* equalling 0.0068, 50.7699, and 5.4588 respectively with an R^2 of 0.23 (n=273). The resulting TF (magenta) is plotted in Fig. 9 at Tair = -10 °C (chosen as a representative solid precipitation Tair, Table 1) along with comparative TFs for the DA and SA. The DA transfer function (green) is site specific for Bratt's Lake (previously unpublished) but is very similar to the multi-site DA curve published by Kochendorfer et al. (2018). For reference, the dashed blue line shows the SA Universal Transfer Function (UTF) published by Kochendorfer et al. (2017b) while the Bratt's Lake site specific SA curve (solid blue) was published by Køltzow et al. (2020) but derived using WMO-SPICE data and procedures (Nitu et al., 2018). Interpolating the curves show that at a gauge height wind speed of 5 m s^{-1} at an air temperature of -10 °C (approximating mean conditions during solid precipitation), the predicted CE for the LPDF, DA, and SA configurations at Bratt's Lake are 0.76, 0.64, and 0.45 respectively. At these specific site conditions, the LPDF improves the catch of solid precipitation by 31% more than a SA configuration. The increase over a DA gauge is approximately 12% under the same conditions. The SA UTF has been shown to produce an under-adjustment when applied to Bratt's Lake SA data (Smith et al., 2020), but for intercomparison purposes, the LPDF TF demonstrates a 19% higher predicted CE at these conditions. Although not shown here, the slope of the fitted LPDF curve does not change at temperatures below -1 °C so that the minimum CE at 5 m s^{-1} is 0.76 and the curve shown in Fig. 9 represents the worst-case scenario for LPDF CE.

https://doi.org/10.5194/egusphere-2026-6470
Preprint. Discussion started: 24 November 2026
© Author(s) 2026. CC BY 4.0 License.



305

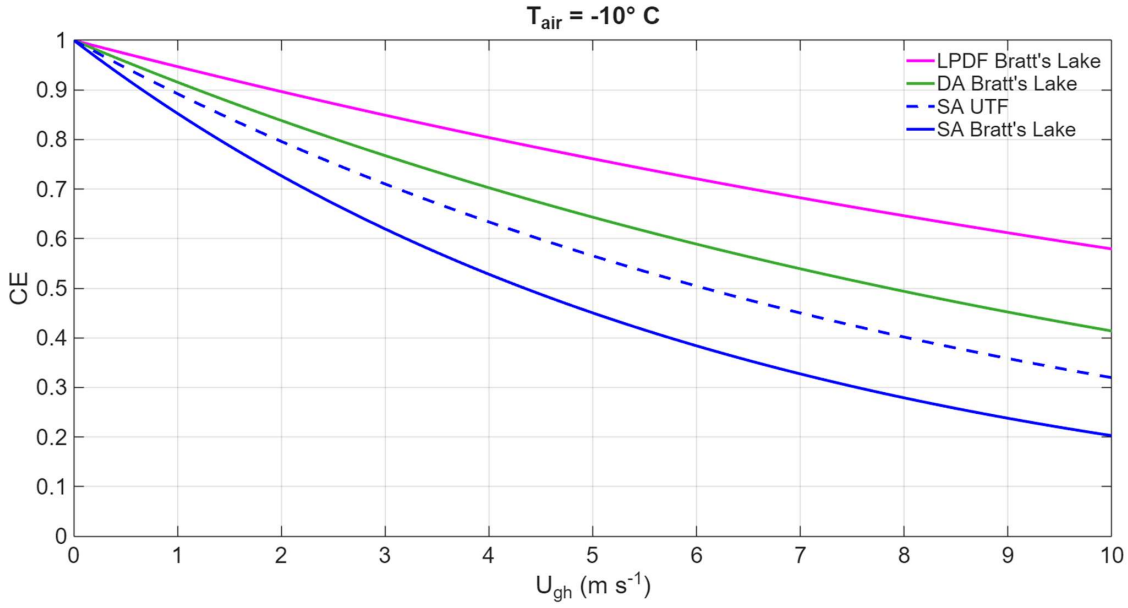

Figure 9: Transfer function curve (Eq. 1) comparison including the Bratt's Lake Low Porosity Double Fence (magenta), the Bratt's Lake Double Alter (green), the Bratt's Lake Single Alter (blue solid) and the WMO-SPICE Single Alter Universal Transfer Function (blue dashed), all derived using an air temperature of -10 °C with wind speed at gauge height.

3.4 Summary and discussion

The intercomparison of the LPDF with the DFAR over three winter seasons at Bratt's Lake indicated that the LPDF wind shield configuration substantially increases the CE of cold season precipitation relative to other commonly used configurations such as the SA and DA. Over the three seasons, the LPDF led to RTC of 74% for solid precipitation, with an increase over the 54% and 61% by the SA and DA configurations respectively. Although Computational Fluid Dynamics (CFD) modelling would be needed for verification (such as that reported by Baghapour et al., 2017), the low wind porosity created by the fence panel inserts, combined with the double fencing, reduces the air flow over the gauge much more effectively than less substantial shielding so that the LPDF caught 20% more precipitation than the SA (when compared to the reference). This is significant for solid precipitation monitoring. Considering that spring runoff on the Canadian Prairies may be reduced to zero when winter precipitation is 15% less than normal (Fang & Pomeroy, 2007), a 20% change in gauge CE (and hence measured winter precipitation amount) could easily impact decisions related to drought monitoring and water resource forecasting. Furthermore, since Bratt's Lake serves as a proxy for assessing gauge configurations for the Arctic (cold and windy conditions and high

https://doi.org/10.5194/egusphere-2026-6470
Preprint. Discussion started: 24 November 2026
© Author(s) 2026. CC BY 4.0 License.

exposure), the same or greater uncertainty related to gauge CE could impact decisions related to infrastructure as well as broader implications for ecosystem research and modelling (Bokhorst et al., 2016). To put this into context, the CMIP5 2031-2050 projected increase for winter precipitation in the Arctic is < 30% (Bush & Lemmen, 2019) which is not substantially higher than the potential increase in gauge CE by using the LPDF.

An additional advantage of the LPDF over the SA and DA configurations is a reduction in the number of hourly periods during which the DFAR records precipitation (> 0 mm) but the less-shielded gauges record no precipitation (0 mm). This advantage, related to increased shielding for detecting light events, was indicated by manual gauge configurations and daily precipitation measurements (Konosuke et al., 2006), but becomes even more important for higher frequency automated measurements (Smith et al., 2020). Over the three seasons at Bratt's Lake, approximately 212 of the 680 hourly periods when the DFAR reported precipitation (~31%) are completely missed by the GeonorSA. This number decreases to 147 periods (~22%) for the LPDF. Although the increase in total measured precipitation by the LPDF by detecting these events is only 3% higher than what the SA detected, these non-zero LPDF measurements make it possible to use a TF to adjust for wind bias thereby pushing the measured LPDF precipitation closer to the true precipitation.

The fitted TF for the LPDF shown in Fig. 9 illustrates the relative increase in CE and the rate that CE decreases with increasing wind speed (at an air temperature of -10 °C) as compared to the P2LDA and GeonorSA at the Bratt's Lake site. Some important considerations need to be noted. Firstly, the slope of the LPDF curve, as fitted with the three seasons of data, does not change with temperatures below -1 °C even though over 65% of the data have a mean temperature < -1 °C. This isn't unlike the behaviour of the fitted curves for the other two configurations (see Smith et al., 2022 as an example for the SA), but the temperature at which the slope of the LPDF TF becomes static is about 4 °C higher than the SA TF for the same site. This could indicate that the aerodynamic impact of the LPDF is as effective at increasing CE at colder temperatures (with smaller and lighter hydrometeors) as it is at warmer temperatures (with larger and heavier hydrometeors), but it might also indicate weaknesses in the fit and that the LPDF TF is not very robust. The latter conjecture is more likely given that the R^2 value of the fit is only 0.28. Therefore, while the LPDF TF shown in Fig. 9 is a useful intercomparison tool and provides decision making guidance on where the LPDF might be beneficial, it would be inadvisable to use this TF for adjusting the precipitation measured by similar shield configurations (especially at other sites) until its robustness and universality can be further proved.

The advantages of the LPDF for increasing the cold season CE of automated precipitation gauge measurements in a Canadian Prairie environment are clear, but this intercomparison failed to demonstrate the same high CE shown by Kochendorfer et al. (2023) vs. the DFAR at Marshall, CO where the LPDF achieved a CE > 0.98. This is a reflection on the measurement conditions at Bratt's Lake where winter precipitation occurs at relatively low temperatures and relatively high wind speeds. In comparison, while more than 95% of "snow days" (defined by K2023 as precipitation > 1 mm and mean air temperature < -2 °C over 24 hours) at Marshall had wind speeds < 5 m s^{-1}, only 57% of snow days at Bratt's Lake occurred at those lower wind speeds. For

https://doi.org/10.5194/egusphere-2026-6470
Preprint. Discussion started: 24 November 2026
© Author(s) 2026. CC BY 4.0 License.

Bratt's Lake hourly solid precipitation events (precipitation > 0 mm and mean air temperature < -2 °C over 60 minutes), less than 47% experience wind speeds < 5 m s^{-1}, illustrating a substantially different measurement environment than any of the NOAA intercomparison sites in the USA. It was not unexpected that the LPDF at Bratt's Lake did not perform as well as it did at Marshall as compared to the DFAR. Unfortunately, because Boulder and Chatham only operated a SDFIR as a reference and not a DFAR, the CE results are not directly comparable

From a cost advantage perspective, the components of the LPDF can be purchased for about $3.5K CAD (~2.2K EUR) and assembled in about a day. The Canadian Double Alter shield (Fig. 4c) can be manufactured in Canada for approximately $5K CAD (~3.1K EUR) and typically assembled in a few hours. The LPDF, therefore, provides a higher CE at a lower cost. However, the LPDF components are bulkier and heavier than those of the Canadian Double Alter, so purchase cost savings may be negated by more expensive shipping and installation costs. Installed footprint is also a consideration. The LPDF requires about 450% more space than a DA configuration, so this might be a concern where available space is restricted. As an advantage, the LPDF requires only about 15% of the footprint and construction cost of a DFAR, while achieving nearly 75% of its performance, and perhaps most importantly it is nearly 100% maintenance free.

4 Conclusions

The LPDF has been shown to improve the total catch of an automated accumulating gauge measuring cold season precipitation by up to 20% more than a SA shield configuration and up to 13% more than a DA shield configuration (as compared to a DFAR) over three seasons at the ECCC Bratt's Lake intercomparison site located on the Canadian Prairies. The site-specific TF, which evaluated the relationship between wind speed, temperature, and CE, showed that at a wind speed of 5 m s^{-1} and an air temperature of -10 °C, the LPDF led to a CE of 0.75 while the SA and DA gauges led to a CE of 0.45 and 0.64, respectively. This finding is a substantial improvement with a relatively low cost while maintaining a moderate footprint. However, the performance of the LPDF in the relatively cold and windy measurement environment of Bratt's Lake was proven to be less favourable than what was shown in previous intercomparisons undertaken in the United States where the LPDF CE was greater than 0.98. The Bratt's Lake assessment suggests that the LPDF could be used in operational or research networks to decrease bias errors in solid precipitation measurements made in harsher winter climates by increasing both the CE and the detectability of light events. However, the LPDF should not be considered as a replacement for the DFAR as a reference configuration for solid precipitation measurement in those same environments. With an RTC for solid precipitation of 74%, the LPDF would require the development and application of a robust transfer function to facilitate the accurate estimation of precipitation where cold and windy conditions are prevalent during winter.

https://doi.org/10.5194/egusphere-2026-6470
Preprint. Discussion started: 24 November 2026
© Author(s) 2026. CC BY 4.0 License.

Code and data availability

The data used in this intercomparison will be available via the Government of Canada Open Government Portal. The NAF-S code used to filter the high frequency "raw" automated precipitation gauge bucket weight data are available at https://doi.org/10.20383/101.0243.

Author contributions

CS helped lead the intercomparison and prepared the results and the manuscript. AR led data collection, archiving, quality control, and filtering and contributed to preparing the manuscript. JK contributed to the original design of the LPDF and provided input for the intercomparison and manuscript revision. CJ sourced LPDF components from Canadian suppliers and led the onsite construction and initial testing.

Competing interests

The authors have no competing interests.

Disclaimer

Copernicus Publications remains neutral with regard to jurisdictional claims made in the text, published maps, institutional affiliations, or any other geographical representation in this paper. While Copernicus Publications makes every effort to include appropriate place names, the final responsibility lies with the authors. Views expressed in the text are those of the authors and do not necessarily reflect the views of the publisher. The scientific results and conclusions, as well as any views or opinions expressed herein, are those of the author(s) and do not necessarily reflect those of OAR or the Department of Commerce.

Copyright statement

The works published in this journal are distributed under the Creative Commons Attribution 4.0 License. This licence does not affect the Crown copyright work, which is re-usable under the Open Government Licence (OGL). The Creative Commons Attribution 4.0 License and the OGL are interoperable and do not conflict with, reduce or limit each other.
© Crown copyright 2026

https://doi.org/10.5194/egusphere-2026-6470
Preprint. Discussion started: 24 November 2026
© Author(s) 2026. CC BY 4.0 License.

Acknowledgements

John Morton and Stephana Stefanyshyn-Alonso contributed to the field site maintenance and data collection while working as University of Saskatchewan co-op students with ECCC.

Review statement

The review statement will be added by Copernicus Publications listing the handling editor as well as all contributing referees according to their status anonymous or identified.

References

Baghapour, B, Sullivan, P.E. : A CFD study of the influence of turbulence on undercatch of precipitation gauges, Atmospheric Research, 197, 265-276, https://doi.org/10.1016/j.atmosres.2017.07.008, 2017.

Barnett, T., Adam, J., Lettenmaier, D.: Potential impacts of a warming climate on water availability in snow-dominated regions, Nature, 438, 303–309, https://doi.org/10.1038/nature04141, 2005.

Bokhorst, S., Pedersen, S.H., Brucker, L. *et al.*: Changing Arctic snow cover: A review of recent developments and assessment of future needs for observations, modelling, and impacts. Ambio, 45, 516–537, https://doi.org/10.1007/s13280-016-0770-0, 2016.

Bush, E. and Lemmen, D.S., editors: Canada's Changing Climate Report, Government of Canada, Ottawa, 444 p., https://changingclimate.ca/CCCR2019 (last accessed October 2026), 2019.

Fang, X., Pomeroy, J.W.: Snowmelt runoff sensitivity analysis to drought on the Canadian prairies, Hydrol. Process., 21: 2594-2609. https://doi.org/10.1002/hyp.6796, 2007.

Goodison, B., Louie, P., and Yang, D.: The WMO solid precipitation measurement intercomparison, World Meteorological Organization-Publications-WMO/TD No. 872, 212 pp, https://library.wmo.int/idurl/4/28336 (last accessed October, 2026), 1998.

Kochendorfer, J., Rasmussen, R., Wolff, M., Baker, B., Hall, M. E., Meyers, T., Landolt, S., Jachcik, A., Isaksen, K., Brækkan, R., and Leeper, R.: The quantification and correction of wind-induced precipitation measurement errors, Hydrol. Earth Syst. Sci., 21, 1973–1989, https://doi.org/10.5194/hess-21-1973-2017, 2017a.

https://doi.org/10.5194/egusphere-2026-6470
Preprint. Discussion started: 24 November 2026
© Author(s) 2026. CC BY 4.0 License.

Kochendorfer, J., Nitu, R., Wolff, M., Mekis, E., Rasmussen, R., Baker, B., Earle, M. E., Reverdin, A., Wong, K., Smith, C. D., Yang, D., Roulet, Y.-A., Buisan, S., Laine, T., Lee, G., Aceituno, J. L. C., Alastrué, J., Isaksen, K., Meyers, T., Brækkan, R., Landolt, S., Jachcik, A., and Poikonen, A.: Analysis of single-Alter-shielded and unshielded measurements of mixed and solid precipitation from WMO-SPICE, Hydrol. Earth Syst. Sci., 21, 3525–3542, https://doi.org/10.5194/hess-21-3525-2017, 2017b.

Kochendorfer, J., Nitu, R., Wolff, M., Mekis, E., Rasmussen, R., Baker, B., Earle, M. E., Reverdin, A., Wong, K., Smith, C. D., Yang, D., Roulet, Y.-A., Meyers, T., Buisan, S., Isaksen, K., Brækkan, R., Landolt, S., and Jachcik, A.: Testing and development of transfer functions for weighing precipitation gauges in WMO-SPICE, Hydrol. Earth Syst. Sci., 22, 1437–1452, https://doi.org/10.5194/hess-22-1437-2018, 2018.

Kochendorfer, J., Earle, M., Rasmussen, R., Smith, C., Yang, D., Morin, S., Mekis, E., Buisan, S., Roulet, Y., Landolt, S., Wolff, M., Hoover, J., Thériault, J. M., Lee, G., Baker, B., Nitu, R., Lanza, L., Colli, M., & Meyers, T.: How well are we measuring snow post-SPICE?. Bulletin of the American Meteorological Society, 103(2), E370-E388. https://doi.org/10.1175/BAMS-D-20-0228.1, 2022.

Kochendorfer, J., Meyers, T. P., Hall, M. E., Landolt, S. D., Lentz, J., and Diamond, H. J.: A new reference-quality precipitation gauge wind shield, Atmos. Meas. Tech., 16, 5647–5657, https://doi.org/10.5194/amt-16-5647-2023, 2023.

Køltzow, M., Casati, B., Haiden, T., Valkonen, T.: Verification of Solid Precipitation Forecasts from Numerical Weather Prediction Models in Norway. Wea. Forecasting, 35, 2279–2292, https://doi.org/10.1175/WAF-D-20-0060.1, 2020.

Lespinas, F., Fortin, V., Roy, G., Rasmussen, P., Stadnyk, T.: Performance evaluation of the Canadian precipitation analysis (CaPA). Journal of Hydrometeorology, 16(5), 2045-2064, https://doi.org/10.1175/JHM-D-14-0191.1, 2015.

Mekis, E., Donaldson, N., Reid, J., Zucconi, A., Hoover, J., Li, Q., Nitu, R., and Melo, S.: An Overview of Surface-Based Precipitation Observations at Environment and Climate Change Canada, Atmos.-Ocean, 56, 71–95, https://doi.org/10.1080/07055900.2018.1433627, 2018.

Nitu, R., Roulet, Y.-A., Wolff, M., Earle, M., Reverdin, A., Smith, C., Kochendorfer, J., Morin, S., Rasmussen, R., Wong, K., Alastrué, J., Arnold, L., Baker, B., Buisán, S., Collado, J. L., Colli, M., Collins, B., Gaydos, A., Hannula, H.-R., Hoover, J., Joe, P., Kontu, A., Laine, T., Lanza, L., Lanzinger, E., Lee, G. W., Lejeune, Y., Leppänen, L., Mekis, E., Panel, J.-M., Poikonen, A., Ryu, S., Sabatini, F., Theriault, J., Yang, D., Genthon, C., van den Heuvel, F., Hirasawa, N., Konishi, H.,

https://doi.org/10.5194/egusphere-2026-6470
Preprint. Discussion started: 24 November 2026
© Author(s) 2026. CC BY 4.0 License.

Nishimura, K., and Senese, A.: WMO Solid Precipitation Intercomparison Experiment (SPICE) (2012–2015), Instruments and Observing Methods Report No. 131, World Meteorological Organization, Geneva, https://library.wmo.int/idurl/4/56317 (last accessed October, 2026), 2018.

Pomeroy, J.W., Gray, D.M., Brown, T., Hedstrom, N.R., Quinton, W.L., Granger, R.J.,Carey, S.K.: The cold regions hydrological model: a platform for basing process representation and model structure on physical evidence. Hydrological Processes, 2667, 2650–2667, https://doi.org/10.1002/hyp.6787, 2007.

Ross, A., Smith, C. D., and Barr, A.: An improved post-processing technique for automatic precipitation gauge time series, Atmos. Meas. Tech., 13, 2979–2994, https://doi.org/10.5194/amt-13-2979-2020, 2020.

Sevruk, B., Hertig, J.-A, Spiess, R.: The effect of precipitation gauge orifice rim on the wind field deformation as investigated in a wind tunnel, Atmosphere Environment, 25A, 1173-1179, https://doi.org/10.1016/0960-1686(91)90228-Y, 1991.

Smith, C. D., Ross, A., Kochendorfer, J., Earle, M. E., Wolff, M., Buisán, S., Roulet, Y.-A., and Laine, T.: Evaluation of the WMO Solid Precipitation Intercomparison Experiment (SPICE) transfer functions for adjusting the wind bias in solid precipitation measurements, Hydrol. Earth Syst. Sci., 24, 4025–4043, https://doi.org/10.5194/hess-24-4025-2020, 2020.

Smith, C. D., Mekis, E., Hartwell, M., and Ross, A.: The hourly wind-bias-adjusted precipitation data set from the Environment and Climate Change Canada automated surface observation network (2001–2019), Earth Syst. Sci. Data, 14, 5253–5265, https://doi.org/10.5194/essd-14-5253-2022, 2022.

Sugiura, K., Ohata, T., Yang, D.: Catch Characteristics of Precipitation Gauges in High-Latitude Regions with High Winds, J. Hydrometeorolgy, **7**, 984–994, https://doi.org/10.1175/JHM542.1, 2006.

Vincent, L. A., Mekis, É.: Changes in daily and extreme temperature and precipitation indices for Canada over the twentieth century, Atmosphere-Ocean, *44*(2), 177–193, https://doi.org/10.3137/ao.440205, 2006.

Vincent, L.A., Zhang, X., Mekis, É., Wan, H., Bush, E.J.: Changes in Canada's climate: Trends in indices based on daily temperature and precipitation data. Atmosphere-Ocean, 56(5), 332-349. https://doi.org/10.1080/07055900.2018.1514579, 2018.

https://doi.org/10.5194/egusphere-2026-6470
Preprint. Discussion started: 24 November 2026
© Author(s) 2026. CC BY 4.0 License.



Wolff, M. A., Isaksen, K., Petersen-Øverleir, A., Ødemark, K., Reitan,T., and Brækkan, R.: Derivation of a new continuous adjustment function for correcting wind-induced loss of solid precipitation: results of a Norwegian field study, Hydrol. Earth Syst. Sci., 19, 951–967, https://doi.org/10.5194/hess-19-951-2015, 2015.

Yang, D., Metcalfe, J. R., Goodison, B. E., and Mekis, E.: True Snowfall. An evaluation of the double fence intercomparison reference gauge, in: 50th Eastern SNOW Conference and 61st Western SNOW Conference, Quebec City, 105–111, https://static1.squarespace.com/static/58b98f7bd1758e4cc271d365/t/5e5d37693e1937250287f0c3/1583167339802/14+D.+Yang%2C+J.R.+Metcalfe%2C+B.E.+Goodison%2C+E.+Mekis.pdf (last accessed October, 2026), 1993.